$$\frac{n_{fv}(A)}{n_{rv}(A)} = \frac{\sigma_A}{\sigma_T\ddagger}$$

as shown earlier by Bishop and Laidler.[8] A similar result may be derived for bimolecular reactions.

References and Notes

(1) S. Glasstone, K. J. Laidler, and H. Eyring, "The Theory of Rate Processes", McGraw-Hill, New York, N.Y., 1941.
(2) P. J. Robinson and K. A. Holbrook, "Unimolecular Reactions", Wiley-Interscience, New York, N.Y., 1972.
(3) (a) J. C. Light, *Discuss. Faraday Soc.*, **44**, 14 (1967); (b) E. Nikitin, *Theor. Exp. Chem. (Engl. Transl.)*, **1**, 83, 90, 275 (1965).
(4) (a) M. A. Eliason and J. O. Hirschfelder, *J. Chem. Phys.*, **30**, 1426 (1959); (b) J. C. Polanyi and J. L. Schreiber, "Physical Chemistry", Vol. VIA, Academic Press, New York, N.Y., 1974, Chapter 6.
(5) The term "reaction pathway" as used by us, and some others,[6,8] is not to be interpreted as being a particular trajectory (or set of trajectories) associated with the classical motion in configuration space. Instead, we view a reaction pathway as an abstract way in which configurations associated with a given reaction may be interconverted. Thus, in a unimolecular reaction a reaction pathway may be associated with a particular stationary point of an activated complex and that of a reactant on the potential energy surface.
(6) E. W. Schlag, *J. Chem. Phys.*, **38**, 2480 (1963).
(7) E. W. Schlag and G. L. Haller, *J. Chem. Phys.*, **42**, 584 (1965).
(8) (a) D. M. Bishop and K. J. Laidler, *J. Chem. Phys.*, **42**, 1688 (1965); (b) *Trans. Faraday Soc.*, **66**, 1685 (1970).
(9) C. S. Elliott and H. M. Frey, *Trans. Faraday Soc.*, **64**, 2352 (1968).
(10) H. S. Johnston, "Gas Phase Reaction Rate Theory", Ronald Press, New York, N.Y., 1966, p 122.
(11) D. Rapp and R. E. Weston, *J. Chem. Phys.*, **36**, 2807 (1962).
(12) V. Gold, *Trans. Faraday Soc.*, **60**, 738 (1964).
(13) R. P. Bell and E. Geller, *Proc. R. Soc. London, Ser. A*, **210**, 310 (1952).
(14) (a) R. A. Marcus, *J. Chem. Phys.*, **43**, 2658 (1965); (b) *ibid.*, **43**, 1598 (1965).

(15) N. Davidson, "Statistical Mechanics", McGraw-Hill, New York, N.Y., 1962, p 149.
(16) K. J. Laidler, "Theories of Chemical Reaction Rates", McGraw-Hill, New York, N.Y., 1969.
(17) M. Gordon and W. B. Temple, *J. Chem. Soc. A*, 729 (1970).
(18) In principle, all of the activated complexes are now in motion toward products. Thus, the value of $[X^\ddagger]$ is actually one-half the previous value requiring that eq 4 be written as $R_r = r^\ddagger v[X^\ddagger]/2$. However, since this error is canceled by one contained in the vibrational factor, kT/hv, the correct result is still obtained. For a logically consistent derivation of rate constants in ART reference should be made to the treatment given by K. G. Denbigh, "The Principles of Chemical Equilibrium", Cambridge University Press, New York, N.Y., 1971, Chapter 15.
(19) J. N. Murrell and K. J. Laidler, *Trans. Faraday Soc.*, **64**, 371 (1968).
(20) A referee has suggested that these conclusions may not be entirely general since an activated complex may also exist when the leading terms in a potential energy function are cubic instead of quadratic. In such a case the region around the critical point resembles three "valleys" converging at a point. Such surfaces are often referred to as "monkey saddles". Activated complexes for such systems may indeed possess more than one mode of decomposition to reactants (≤ 2, in fact) consistent with $r^\ddagger \leq 2$. However, $r^\ddagger$ values greater than 2 are also possible if one *allows* for valley bifurcations[23] or branching points at surface points lower in energy than the critical point. Thus, the conclusion remains that the overall frequency of return to reactants of such complexes is determined by the character of the reaction surface in the immediate vicinity of the critical point and not by the value of $r^\ddagger$. Also, a factor of 2 included in R_r would cancel in the final rate associated with product formation, R_p, since $R_r = 2R_p$ in this case. Because of the relative rarity of "monkey saddles" in reaction systems,[21] we have considered the quadratic approximation adequate for this treatment of statistical factors.
(21) R. E. Stanton and J. W. McIver, Jr., *J. Am. Chem. Soc.*, **97**, 3632 (1975).
(22) J. N. Murrell and G. L. Pratt, *Trans. Faraday Soc.*, **66**, 1680 (1970).
(23) A "valley bifurcation" exists when two "valleys" merge into one on the reaction potential energy surface.
(24) (a) E. Wigner, *J. Chem. Phys.*, **5**, 720 (1937); (b) J. Horiuti, *Bull. Chem. Soc. Jpn.*, **13**, 210 (1938).
(25) (a) J. C. Keck, *Adv. Chem. Phys.*, **13**, 85 (1967); (b) J. C. Keck, *J. Chem. Phys.* **32**, 1035 (1960).

Vibronic Coupling Model for Calculation of Mixed Valence Absorption Profiles

Susan B. Piepho,[*1] **Elmars R. Krausz, and P. N. Schatz**

Contribution from the Department of Chemistry, University of Virginia, Charlottesville, Virginia 22901. Received October 3, 1977

Abstract: A vibronic coupling model for mixed valence systems is developed which provides explicit eigenvalues and eigenfunctions based on the formalism previously developed by Fulton and Gouterman to discuss the excited states of symmetrical dimers. The mixed valence (intervalence) absorption profile is obtained by calculating transition intensities from populated vibronic levels to all higher vibronic levels within the manifold. The parameters of the model are directly related to properties of the "monomeric" units. The theory is first applied to the case of two identical and pseudooctahedral constituent units ("monomers") assuming equal force constants in both oxidation states of the monomer. A number of synthetic profiles are presented for a range of parameters. The unique Creutz–Taube complex ($[(NH_3)_5Ru\text{-}pyr\text{-}Ru(NH_3)_5]^{5+}$) is singled out for analysis. The room temperature absorption spectrum is fit well by a pair of quite closely defined parameters. These parameters indicate that the lower potential surface has a small (~ 57 cm^{-1}) barrier ("valence trapping"). *However*, the lowest vibronic state is calculated to be about 30 cm^{-1} above the top of this barrier. Furthermore, the calculated probability distribution in configuration space shows complete valence delocalization (no trapping) at low temperature, but there is a small hint of trapping at room temperature. The model is extended to unsymmetrical mixed valence systems (nonidentical "monomers"). The consequences both of including spin–orbit coupling and allowing unequal force constants are examined.

I. Introduction

Systems containing ions in two different oxidation states often have intense absorption bands which cannot be attributed to the absorption of either constituent ion. The classic example is Prussian blue, an insoluble crystalline solid containing both six-coordinate ferricyanide [Fe(III)–C–N coordination] and six-coordinate ferrocyanide (Fe(II)–N–C coordination) in a regular cubic array.[2a] Neither of these monomeric species alone gives rise to the intense blue color which apparently results from excitations involving *both* the Fe(II) and Fe(III)

centers. Such transitions are termed mixed valence or intervalence transitions.[2b,c]

In recent years, a new mixed valence complex,

$$[(NH_3)_5RuN\bigcirc NRu(NH_3)_5]^{5+}$$

has been synthesized by Creutz and Taube.[3] This ion is particularly interesting theoretically because the two Ru atoms have identical coordination spheres but different oxidation states; one is Ru(II) and the other Ru(III). In the visible absorption region the Creutz–Taube (C–T) complex shows the

spectrum typical of analogous Ru(II)-Ru(II) complexes, but in the near-infrared region, a new absorption band appears which is unique to the Ru(II)-Ru(III) complex.[3a] This mixed-valence transition is lower in energy, sharper, and much more asymmetric than mixed-valence bands in less symmetrical complexes. It was partly the unusual bandshape of the C-T ($\equiv$ Creutz-Taube) absorption which stimulated the present study.

The theory most frequently cited to explain mixed-valence intensity is that of Hush.[4-7] Hush's theory has not, however, been used to calculate absorption profiles. A rigorous approach to the problem of mixed valence intensities is to determine the energies of the complete manifold of vibronic states of the complex and then to calculate intensities of transitions from the populated low-lying vibronic levels to all higher vibronic states. This may be accomplished surprisingly easily using the approximate method of Fulton and Gouterman (F-G).[8,9] The method was developed to calculate the vibronic manifold in the ("Davydov split") excited states of symmetrical dimers. These authors have written two very useful papers on such systems and we follow their general approach. Our system differs substantially from theirs, however, in that the ground state is comprised of all populated vibronic levels *within* our manifold while F-G's ground state is *outside* their manifold of dimer excited-state vibronic levels. *Thus while the relative energies of vibronic levels in our manifold and F-G's are the same, their intensities bear absolutely no relation to ours.* We are considering transitions within the vibronically coupled manifold. Our system corresponds to transitions *between* the "Davydov split" components of F-G's excited states.

II. Theoretical Model. The Symmetrical Limit, A = B

Our system (A–B) in the symmetrical (A = B) limit consists of molecules or ions made up of units A and B whose nuclei go into one another under a symmetry operation. The C-T complex is an example of such a system. We term A and B the monomers and A–B the dimer. The interaction between A and B is assumed small, so it is convenient to write the Hamiltonian for the system in the form

$$H^T = H^A + H^B + V^{AB}(r,Q) + T_n^{AB} \quad (1)$$

where

$$\begin{aligned} H^A &= T_n^A + T_e^A + V(r_A,Q_A) \\ H^B &= T_n^B + T_e^B + V(r_B,Q_B) \end{aligned} \quad (2)$$

Here the T_n and T_e operators are nuclear and electronic kinetic energy operators, the V are potential energy operators, and r and Q refer respectively to electronic and nuclear coordinates. $V^{AB}(r,Q)$ represents all interaction terms between A and B while T_n^{AB} is the kinetic energy operator for their relative motion.

We first consider eq 1 holding the nuclei at their equilibrium positions (Q^0) assuming that $V^{AB}(r,Q^0)$ is sufficiently small to be neglected; it is subsequently treated perturbationally. Thus eq 1 is separable in r_A and r_B, and solutions will be products of H^A and H^B solutions,

$$\psi_k(r,Q^0) = \psi_R^A(r_A,Q_A^0)\psi_S^B(r_B,Q_B^0) \quad (3)$$

where ψ_R^A and ψ_S^B are eigenstates of H^A and H^B, respectively.

There are two equivalent ways to make the division of eq 1 into H^A and H^B, since in our symmetrical mixed valence system, A and B differ only in oxidation state. Thus, suppose first that A is in the higher oxidation state M (e.g., Ru(III)) with ground state ψ_M^A while B is in the lower oxidation state N (e.g., Ru(II)) with ground state ψ_N^B. In this case the zeroth-order solution to eq 1 is

$$\psi_a(r,Q^0) = \psi_M^A\psi_N^B \quad (4)$$

Alternatively, however, we could have A in the lower oxidation state N and B in the higher oxidation state M to give the zeroth-order solution

$$\psi_b(r,Q^0) = \psi_N^A\psi_M^B \quad (5)$$

These states are exactly degenerate and go into one another under exchange of A and B. We use them as our electronic basis states and neglect interactions with electronic states outside of this basis. We further make the approximation

$$\langle \psi_a | \psi_b \rangle \simeq 0 \quad (6)$$

This integral is proportional to the overlap of orbitals centered on A with those centered on B and so is zero in the one-center approximation. (In the F-G problem, eq 6 is exactly true.)

Note that at this point ψ_a and ψ_b are exactly degenerate so we cannot even talk about a purely electronic mixed valence transition between them. Inclusion of the $V^{AB}(r,Q)$ perturbation *and* at least an approximate solution of the vibronic Hamiltonian eq 1 are *both* required before an absorption band with any intensity is calculated. We show later that treating $V^{AB}(r,Q)$ as a purely electronic exciton coupling term and neglecting vibronic interactions leads to the prediction of a single line. Alternatively, ignoring exciton coupling and including vibronic interactions leads to the prediction of zero intensity.

We now seek an approximate solution to eq 1. We make the harmonic approximation and, for reasons explained subsequently, we assume a single totally symmetric vibrational degree of freedom for each monomer. The unperturbed vibronic wave functions associated with our zero-order H^A and H^B eigenfunctions are thus

$$\psi_M^A(r_A,Q_A' = 0)\chi'_{mA}(Q_A)$$
$$\psi_N^A(r_A,Q_A = 0)\chi_{nA}(Q_A)$$
$$\psi_M^B(r_B,Q_B' = 0)\chi'_{mB}(Q_B)$$
$$\psi_N^B(r_B,Q_B = 0)\chi_{nB}(Q_B) \quad (7)$$

where $\chi_{nA}(Q_A)$ and $\chi'_{nA}(Q_A)$, for example, are the harmonic oscillator solutions to

$$\left[\frac{P_A^2}{2M_A} + W_N^A(Q_A = 0) + \frac{1}{2}k_N^A Q_A^2\right] \\ \times \chi_{nA}(Q_A) = E_{nA}\chi_{nA}(Q_A) \quad (8)$$

and

$$\left[\frac{P_A^2}{2M_A} + W_M^A(Q_A = 0) + \ell_M^A Q_A \right. \\ \left. + \frac{1}{2}k_M^A Q_A^2\right] \chi'_{nA}(Q_A) = E'_{nA}\chi'_{nA}(Q_A) \quad (9)$$

respectively. Here $T_n^A = P_A^2/2M_A$ and the other terms in brackets describe the harmonic potentials for ψ_N^A and ψ_M^A. Thus, for example,

$$W_M^A(Q_A) = W_M^A(Q_A = 0) + \ell_M^A Q_A + \frac{1}{2}k_M^A Q_A^2 \quad (10)$$

is the potential for ψ_M^A; i.e.,

$$[T_e^A + V(r_A,Q_A)]\psi_M^A = W_M^A(Q_A)\psi_M^A \quad (11)$$

and $W_M^A(Q_A)$ is assumed harmonic, and so forth for the other cases. The potentials and notation are displayed in Figure 1. We assume an identical force constant $k = k_N = k_M$ for ψ_M^A and ψ_N^A. Analogous equations hold for B. Note that we have chosen our monomer normal coordinates so that $Q_A = 0$ at the potential minimum of ψ_N^A and $Q_B = 0$ at the minimum of ψ_N^B. This choice is arbitrary. The minimum of ψ_M^A (e.g., Ru(III)) will not in general fall at the same point in Q_A space as that for

ψ_N^A (Ru(II)) so the equation for the $\chi'_{nA}(Q_A)$ is that of a displaced harmonic oscillator with respect to that for the $\chi_{nA}(Q_A)$. If Q_A were not totally symmetric, movement of the minimum away from $Q_A = 0$ would correspond to a different monomer symmetry in states ψ_N^A and ψ_M^A. We make the assumption that the monomer has the same symmetry in the two oxidation states and so only totally symmetric Q_A (Q_B) give ℓ^A (ℓ^B) $\neq$ 0 in eq 10. We show subsequently that modes with $\ell^A = 0$ add nothing significant to the mixed valence problem in our approximation. Thus, our limitation to a single, totally symmetric vibrational degree of freedom per monomer is not as restrictive as it might first appear.

We now construct the vibronic matrix for eq 1 in our zero-order electronic basis, ψ_a and ψ_b. The basis is diagonal in and commutes with T_n^A, T_n^B, and T_n^{AB}. We follow F–G[8,9] and approximate $V^{AB}(r,Q)$ by expanding it in a Taylor series about $Q = Q^0$ keeping only the constant terms:

$$W^{AB} \simeq W^{AB}(q,Q^0) \equiv \langle \psi_a | V^{AB}(r,Q^0) | \psi_a \rangle$$
$$= \langle \psi_b | V^{AB}(r,Q^0) | \psi_b \rangle \quad (12)$$

and

$$W_s \simeq W_s(q,Q^0) \equiv \langle \psi_a | V^{AB}(r,Q^0) | \psi_b \rangle$$
$$= \langle \psi_b | V^{AB}(r,Q^0) | \psi_a \rangle \quad (13)$$

Thus in our approximation W^{AB} is a constant term along the diagonal and W_s is a purely electronic, exciton coupling parameter. (In an exact treatment W_s would depend on the coordinates of relative motion of A and B (the Q_{AB}); W^{AB} would depend on the Q_{AB} and, probably to a lesser extent, on the Q_A and Q_B.) The vibronic Hamiltonian, expressed as a matrix in our zeroth-order ψ_a, ψ_b electronic basis, is thus

$$
\begin{bmatrix}
\left\{ \dfrac{P_A^2}{2M_A} + W_M^A + \ell_M^A Q_A \right. & \\
\quad + \dfrac{1}{2} k_M^A Q_A^2 + \dfrac{P_B^2}{2M_B} + W_N^B & W_s \\
\quad + \dfrac{1}{2} k_N^B Q_B^2 + T_n^{AB} + W^{AB} \Big\} & \\
& \left\{ \dfrac{P_A^2}{2M_A} + W_N^A + \dfrac{1}{2} k_N^A Q_A^2 \right. \\
W_s & \quad + \dfrac{P_B^2}{2M_B} + W_M^B + \ell_M^B Q_B \\
& \quad + \dfrac{1}{2} k_M^B Q_B^2 + T_n^{AB} + W^{AB} \Big\}
\end{bmatrix}
$$

$$(14)$$

We shall find with our approximations that vibronic coupling arises only through the terms $\ell_M^A Q_A$ and $\ell_M^B Q_B$ above. In the symmetrical case we may write $\ell = \ell_M^A = \ell_M^B$ and we assume that $k_N = k_M$ so that $k = k_M^A = k_N^A = k_M^B = k_N^B$.
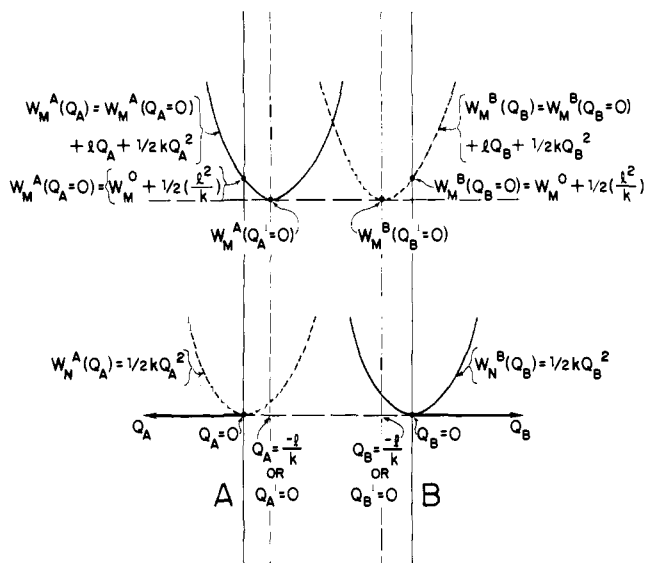
To exploit the symmetry of the system we now transform to the set of dimer normal coordinates

$$Q_\pm = \frac{1}{\sqrt{2}} (Q_A \pm Q_B) \quad (15)$$

and to the set of electronic functions

$$\psi_\pm(r,Q^0) = \frac{1}{\sqrt{2}} (\psi_a \pm \psi_b) \quad (16)$$

The vibronic Hamiltonian of eq 14 rewritten in the ψ_+, ψ_- electronic basis gives

Figure 1. A schematic diagram of the potential surfaces for $\psi_a = \psi_M^A \psi_N^B$ (solid line) and $\psi_b = \psi_N^A \psi_M^B$ (dashed line) in the symmetrical (A = B) limit. We choose our energy scale so that $E = W_N^A(Q_A = 0) = W_N^B(Q_B = 0) = 0$. We abbreviate $\ell \equiv \ell_M^A = \ell_M^B$ and $k \equiv k_M^A = k_N^A = k_M^B = k_N^B$. The diagram is drawn for the case in which equilibrium bond lengths are longer in the lower oxidation state N and where the lower oxidation state N is lower in energy than the higher oxidation state M. Both conditions apply to the Creutz-Taube complex but not necessarily for other systems.

$$
\begin{bmatrix}
\left\{ \dfrac{P_+^2}{2M} + \dfrac{\ell}{\sqrt{2}} Q_+ + \dfrac{1}{2} k Q_+^2 \right. & \\
\quad + \dfrac{P_-^2}{2M} + \dfrac{1}{2} k Q_-^2 \Big\} + W_s & \dfrac{\ell}{\sqrt{2}} Q_- \\
& \\
& \left\{ \dfrac{P_+^2}{2M} + \dfrac{\ell}{\sqrt{2}} Q_+ + \dfrac{1}{2} k Q_+^2 \right. \\
\dfrac{\ell}{\sqrt{2}} Q_- & \quad + \dfrac{P_-^2}{2M} + \dfrac{1}{2} k Q_-^2 \Big\} - W_s
\end{bmatrix}
$$

$$(17)$$

where we have dropped W_M^A, W_N^A, W_M^B, W_N^B, W^{AB}, and T_n^{AB} since, with respect to the vibronic and electronic coupling, they are constant terms along the diagonal.

We are now ready to solve this matrix to obtain vibronic eigenfunctions for the A–B dimer. With the transformations of eq 15 and 16, the obvious vibrational basis to use is that of the $\chi_{n+}(Q_+)$ and $\chi_{n-}(Q_-)$, the harmonic oscillator solutions to

$$\left[\frac{P_+^2}{2M} + \frac{1}{2} k Q_+^2 \right] \chi_{n+}(Q_+) = \left[\left(n_+ + \frac{1}{2} \right) h\nu_+ \right] \chi_{n+}(Q_+)$$

$$(18)$$

and

$$\left[\frac{P_-^2}{2M} + \frac{1}{2} k Q_-^2 \right] \chi_{n-}(Q_-) = \left[\left(n_- + \frac{1}{2} \right) h\nu_- \right] \chi_{n-}(Q_-)$$

$$(19)$$

respectively.

This *enormously simplifies* the vibronic problem in comparison with using the basis of eq 7. The problem is separable with respect to Q_+ and Q_-. The Q_+ solutions, the $\chi_{n+}(Q_+)$, are simply those of a displaced harmonic oscillator since $(\ell/\sqrt{2})Q_+$ appears only along the diagonal. When $k_N = k_M$, the Q_+ do not couple our electronic basis functions (see eq 17).

They are therefore not involved in any intensity mechanism for the mixed valence transitions (see section III), and we drop them. Thus the only matrix we need solve is the Q_- matrix in the $\chi_{n-}(Q_-)$ basis. We rewrite the matrix in terms of the dimensionless variables

$$q_- = 2\pi(M\nu_-/h)^{1/2}Q_-$$

$$p_- = (Mh\nu_-)^{-1/2}P_-$$

$$\lambda = (8\pi^2Mh\nu_-^3)^{-1/2}\ell$$

$$\epsilon = W_s/h\nu_- \tag{20}$$

so that all energies and parameters are in units of the $\chi_{n-}(q_-)$ vibrational quanta, $h\nu_-$. We henceforth write $n = n_-$ and $h\nu = h\nu_-$ to simplify our notation. Thus our vibronic matrix for $H^T/h\nu$ in the ψ_+,ψ_- basis becomes

$$\begin{bmatrix} \frac{1}{2}(p_-^2 + q_-^2) + \epsilon & \lambda q_- \\ \\ \lambda q_- & \frac{1}{2}(p_-^2 + q_-^2) - \epsilon \end{bmatrix} \tag{21}$$

from which it is straightforward to obtain the matrix in the vibronic basis $\psi_\pm\chi_n(q_-)$, $n = 0, 1, 2, \ldots$.

Since the only nonzero integrals for q_- between our harmonic oscillator functions $\chi_n(q_-)$ are

$$\langle\chi_n|q_-|\chi_{n+1}\rangle = \langle\chi_{n+1}|q_-|\chi_n\rangle = \left(\frac{n+1}{2}\right)^{1/2}$$
$$n = 0, 1, 2, \ldots \tag{22}$$

and since in the symmetrical limit there are no other off-diagonal matrix elements, the matrix blocks into Φ^- and Φ^+ parts where the superscript designates behavior under interchange of nuclei. The Φ^- block is composed of the $\psi_+\chi_n(q_-)$, $n = 1, 3, 5, \ldots$, and the $\psi_-\chi_n(q_-)$, $n = 0, 2, 4, \ldots$, while the Φ^+ block is made up of the $\psi_+\chi_n(q_-)$, $n = 0, 2, 4, \ldots$, and the $\psi_-\chi_n(q_-)$, $n = 1, 3, 5, \ldots$. Diagonal elements are

$$\left\langle \psi_\pm\chi_n(q_-) \left|\frac{H^T}{h\nu}\right| \psi_\pm\chi_n(q_-) \right\rangle = n + \frac{1}{2} \pm \epsilon \tag{23}$$

where $+\epsilon$ applies for the ψ_+ and $-\epsilon$ for the ψ_-. The dimension of the blocks for a basis of $(m - 1)$ quanta is only $m \times m$. Moreover, the blocks may be easily arranged into tridiagonal form, and thus they are very inexpensive to diagonalize. It is therefore possible to include a sufficiently large number of quanta so that the results are insensitive to the truncation from $n = \infty$. Consequently, *essentially exact* results may be obtained within the context of the model.

III. Intensity Profile of the Mixed Valence Band in the Symmetrical Limit

Eigenfunctions for the Φ^+ and Φ^- blocks will be in the form

$$\Phi_\nu^+ = \sum_{n=0,2,4\ldots} r_{\nu n}\psi_+\chi_n + \sum_{n=1,3,5\ldots} r_{\nu n}\psi_-\chi_n$$

$$\Phi_\nu^- = \sum_{n=1,3,5\ldots} s_{\nu n}\psi_+\chi_n + \sum_{n=0,2,4\ldots} s_{\nu n}\psi_-\chi_n \tag{24}$$

with Φ_0^+ lying lowest for negative values of ϵ. Symmetry selection rules allow only + to − or − to + vibronic transitions. Assuming a collection of randomly oriented molecules, the dipole strength of a vibronic line, $\Phi_{\nu'}^+ \rightarrow \Phi_\nu^-$, is given by

$$D(\nu' \rightarrow \nu) = \sum_{\gamma=x,y,z} \frac{(N_{\nu'} - N_\nu)}{N} |\langle\Phi_{\nu'}^+|m_\gamma|\Phi_\nu^-\rangle|^2 \tag{25}$$

where $N_{\nu'}/N$ is the fractional population in state ν'. $N_{\nu'} = \exp(-E_{\nu'}/kT)$ and $N = \sum_{\nu'}N_{\nu'}$. $m_\gamma(\gamma = x, y, \text{or } z)$ is the γth

component of the molecule-fixed electric-dipole operator, $\boldsymbol{m} = \Sigma_i e_i \boldsymbol{r}_i$. The $\boldsymbol{r}_i$ are measured from the midpoint of A and B or, since we center A and B on the z axis, from $z = 0$. The mixed valence band will consist of the totality of such "lines", each centered at its transition energy.

We assume for the moment that ψ_+ and ψ_- are nondegenerate and that the temperature is low enough so that only Φ_0^+ is appreciably populated. Then, making the franck-Condon approximation, we obtain

$$D(0^+ \rightarrow \nu^-) = \sum_{\gamma=x,y,z,} |\langle\Phi_0^+|m_\gamma|\Phi_\nu^-\rangle|^2$$

$$= \sum_{\gamma=x,y,z} \left| \left\{ \langle\psi_+|m_\gamma|\psi_-\rangle \sum_{n=0,2,\ldots} r_{0n}s_{\nu n} \right.\right.$$
$$\left.\left. + \langle\psi_-|m_\gamma|\psi_+\rangle \sum_{n=1,3,\ldots} r_{0n}s_{\nu n} \right\} \right|^2 \tag{26}$$

When ψ_a, ψ_b and γ are real, eq 26 gives

$$D(0^+ \rightarrow \nu^-) = \sum_{\gamma=x,y,z} \left|\langle\psi_+|m_\gamma|\psi_-\rangle \sum_n r_{0n}s_{\nu n}\right|^2$$

$$= \mathscr{S}_{0\nu}^2 \sum_{\gamma=x,y,z} |\langle\psi_+|m_\gamma|\psi_-\rangle|^2 \tag{27}$$

The last line defines the vibrational overlap factors, $\mathscr{S}_{0\nu}$, as

$$\mathscr{S}_{0\nu} = \sum_n r_{0n}s_{\nu n} \tag{28}$$

We now demonstrate that only $m_\gamma = m_z$ polarized electric-dipole transitions are allowed to a first approximation. In the one-center approximation

$$\langle\psi_+|m_\gamma|\psi_-\rangle = \frac{1}{2}\langle\psi_a + \psi_b|m_\gamma|\psi_a - \psi_b\rangle$$

$$\simeq \frac{1}{2}\{\langle\psi_a|m_\gamma|\psi_a\rangle - \langle\psi_b|m_\gamma|\psi_b\rangle\}$$

$$= \frac{1}{2}\{\langle\psi_M^A\psi_N^B|m_\gamma|\psi_M^A\psi_N^B\rangle - \langle\psi_N^A\psi_M^B|m_\gamma|\psi_N^A\psi_M^B\rangle\} \tag{29}$$

Transforming the operator to the monomer centers gives

$$m_x = m_x^A, \; m_y = m_y^A, \; m_z = m_z^A - \frac{Re}{2}$$
$$m_x = m_x^B, \; m_y = m_y^B, \; m_z = m_z^B + \frac{Re}{2} \tag{30}$$

where R is the distance between the monomer centers and e is the electronic charge. Thus if the M state contains m electrons and the N state n electrons,

$$\langle\psi_M^A\psi_N^B|m_z|\psi_M^A\psi_N^B\rangle$$
$$= \left\langle \psi_M^A\left|m_z^A - \frac{Re}{2}\right|\psi_M^A \right\rangle + \left\langle \psi_N^B\left|m_z^B + \frac{Re}{2}\right|\psi_N^B \right\rangle$$
$$\simeq \left(\frac{n-m}{2}\right)Re\langle\psi_N^A\psi_M^B|m_z|\psi_N^A\psi_M^B\rangle \simeq -\left(\frac{n-m}{2}\right)Re \tag{31}$$

All m_γ^A and m_γ^B (and hence m_x and m_y) integrals are zero to a first approximation if the monomer units have approximate inversion symmetry as do the near-octahedral monomers in the C-T complex and in many other complexes. This result follows from parity selection rules. In such systems m_γ^A and m_γ^B ($\gamma = x, y,$ and z) are odd under inversion and can only connect monomer functions which differ in parity.

Thus to summarize, when $n - m = 1$,

$$\langle\psi_+|m_z|\psi_-\rangle \simeq Re/2$$
$$\langle\psi_+|m_x|\psi_-\rangle \simeq 0$$
$$\langle\psi_+|m_y|\psi_-\rangle \simeq 0 \tag{32}$$
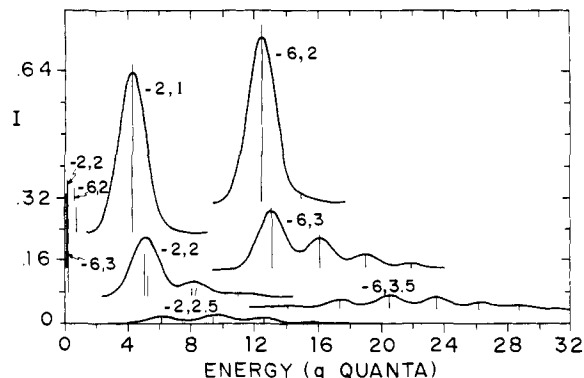
Figure 2. Calculated absorption profiles for the symmetrical case in the low temperature limit. The parameters $-\epsilon,\lambda$ label the transitions. The height of each stick is $\mathscr{S}_{0\nu}^2/2$ (see eq 28), and the curves are synthesized (eq 36) from Gaussians (eq 35) taking all $\Delta = 1.2$. All spectra are on the same intensity scale with vertical displacements for clarity. The very low energy infrared transitions for $-2,2.5$ and $-6,3.5$, which would occur at zero energy to the scale of the figure, have been omitted.

and so when only Φ_0^+ is populated and $\psi_\pm$ are nondegenerate, we obtain

$$D(0^+ \to \nu^-) = |\langle \psi_+|m_z|\psi_-\rangle|^2 \mathscr{S}_{0\nu}^2 = (Re/2)^2 \mathscr{S}_{0\nu}^2 \qquad (33)$$

thus the relative intensities of the lines comprising the band are determined by the $\mathscr{S}_{0\nu}^2$. In section VI we consider how eq 33 is altered in the more general case.

To obtain a qualitative feel for the bandshape changes as a function of ϵ and λ, we first consider the $\mathscr{S}_{0\nu}$ for limiting cases. When $\lambda = \epsilon = 0$

$$\mathscr{S}_{0\nu} = \delta_{0\nu} \qquad (34)$$

(see also section IX), but no mixed valence band is predicted since $\Phi_0^+ = \psi_+\chi_0(q_-)$ and $\Phi_0^- = \psi_-\chi_0(q_-)$ are exactly degenerate. When $\lambda = 0$ but $\epsilon \neq 0$, we still have $\mathscr{S}_{0\nu} = \delta_{0\nu}$, but $\Phi_0^+ = \psi_+\chi_0(q_-)$ and $\Phi_0^- = \psi_-\chi_0(q_-)$ are separated in energy by 2ϵ. Thus a single line is predicted at an energy of 2ϵ. Finally, when $\lambda \neq 0$ but $\epsilon = 0$, we again find $\mathscr{S}_{0\nu} = \delta_{0\nu}$. (In this case, $\Phi_0^+ = \psi_+\chi_0'(q_-)$ and $\Phi_0^- = \psi_-\chi_0'(q_-)$ where $\chi_0'(q_-)$ is the $n = 0$ state for a displaced oscillator in q_-.) Since the states are exactly degenerate with energies $n + \frac{1}{2} - \frac{1}{2}\lambda^2 = \frac{1}{2} - \frac{1}{2}\lambda^2$, no mixed-valence band is predicted.

Clearly, the interesting results occur when both ϵ and λ are nonzero and we no longer have $\mathscr{S}_{0\nu} = \delta_{0\nu}$. In Figure 2, we illustrate the bandshapes predicted by eq 33 for a variety of ϵ,λ combinations. The spectra have been synthesized assuming a Gaussian line shape

$$f_\ell(E) = \frac{\exp[-(E - E_\ell)^2/\Delta^2]}{\Delta\sqrt{\pi}} \qquad (35)$$

with the same Δ value for each vibronic line contributing to the band. Here E_ℓ is the calculated energy for the line and Δ is a line width chosen empirically to fit a spectrum. The figures represent $\mathscr{S}_\ell^2 \equiv \mathscr{S}_{0\nu}^2$ so they are independent of $|\langle \psi_+|m_z|\psi_-\rangle|^2$. The vertical scale is chosen so that the height of each line in the stick spectra equals $\frac{1}{2}\mathscr{S}_{0\nu}^2 = \frac{1}{2}\mathscr{S}_\ell^2$ and the curves represent

$$\sum_\ell \mathscr{S}_\ell^2 f_\ell(E) \qquad (36)$$

In general, we see that a band spanning a small number of quanta centered at an energy near 2ϵ results when ϵ is large compared to λ. In contrast, when λ is large compared to ϵ, the infrared has a very strong transition between nearly degenerate Φ_0^+ and Φ_0^- states, and higher energy excitations give a much broader and weaker band to higher energy. When λ is small compared to ϵ, the lowest lying $\Phi_0^+ \to \Phi_\nu^-$ excitations are es-
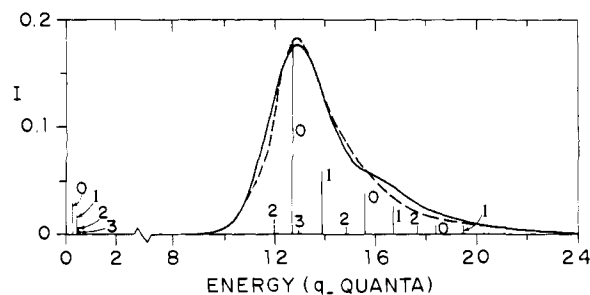
Figure 3. The Creutz–Taube spectrum (dashed curve) at room temperature (from ref 3a) scaled in intensity to the "best fit" of the model (solid curve) which uses $\epsilon = -6$, $\lambda = 2.7$; $\Delta = 1.4$ for all lines. The calculated height of each stick is $\mathscr{S}_{\ell\nu}^2/2$ scaled by the appropriate normalized population factor based on $T = 298$ K. The labels 0, 1, 2, 3 designate transitions from the ground and first three hot vibronic levels, respectively. The energy of a q_- quantum is 500 cm^{-1}.

sentially infrared transitions in ν_- which become allowed as the ψ_+ and ψ_- states are mixed via λq_-. The most intense is the $\Phi_0^+ \to \Phi_0^-$ transition. For $\lambda \to 0$ this is a $\psi_+\chi_0(q_-) \to \psi_+\chi_1(q_-)$ transition with energy $h\nu_-$ and zero intensity. For a given ϵ these transitions become more intense but lower in energy as λ increases. At a given temperature, for λ sufficiently large compared to ϵ, Φ_0^- becomes thermally populated and induced emission must be included in the calculation of the intensity of $\Phi_0^+ \to \Phi_0^-$.

These low-energy infrared transitions should be unique to the mixed valence complexes since to a first approximation their intensity is dependent on the existence of two distinct types of electronic states, ψ_a and ψ_b, which are degenerate to zero order and are coupled by λ. The Ru(II)–Ru(II) or Ru(III)–Ru(III) complexes, for example, will have ground states of the type $\psi_g = \psi_N^A\psi_N^B$ and $\psi_{g'} = \psi_M^A\psi_M^B$, respectively; in each complex only *one type* of electronic ground state exists.

The ease of detection of the ν_--type infrared transitions will depend on their energy, intensity, and line width. We shall discuss these transitions in more detail elsewhere.[18]

IV. The Creutz–Taube (C–T) Complex

The mixed valence band in the C–T complex is relatively narrow and rather asymmetric in solution at room temperature;[3a] it becomes somewhat sharper and markedly more asymmetric at 10 K in a poly(vinyl alcohol) foil.[10] In Ru(NH$_3$)$_6^{3+}$, ν_1(a$_{1g}$) = 500 cm^{-1},[13] so we take $\nu_- = 500$ cm^{-1} as the energy of the vibrational quanta in the $\chi_n(Q_-)$ basis (eq 19). Our parameters and eigenvalues are expressed in units of $h\nu_-$ quanta; thus for $\nu_- = 500$ cm^{-1}, $\epsilon = -6$ corresponds to -3000 cm^{-1}, etc.

In Figure 3 we show the spectrum of the C–T complex in D$_2$O at room temperature taken from Figure 2 of ref 3a. Superimposed we show our "best fit" obtained by trial and error. Our fit gives the parameters $\epsilon = -6.0 \pm 0.1$, $\lambda = 2.7 \pm 0.2$ (with $\Delta \approx 1.4$ for all lines). With these parameters, the model predicts low-lying excited states at 131, 362, and 613 cm^{-1}, and transitions from these thermally populated levels ("hot lines") are seen (Figure 3) to make an appreciable contribution to the overall band profile. The theoretical spectrum is seen to fit quite well, and so our model is able to account for an asymmetric bandshape in which the intensity is concentrated over a relatively few quanta. Furthermore, the parameters ϵ and λ are surprisingly well defined by a rather broad and nondescript band. ϵ depends primarily on the transition energy maximum and hence can be fixed quite reliably. λ is determined by the broadness and asymmetry of the band (see Figure 2). The error bounds we quote for λ (2.5–2.9) are in fact quite generous. Theoretical spectra generated using these extremes

differ *markedly* from experiment, being much too sharp and symmetrical for the lower bound and far too broad and asymmetric for the upper bound.

ϵ and λ values are best determined by a moment analysis (see Appendix) which is less dependent on assumptions about line shapes. However, such an analysis requires an accurate and complete band contour with a reliably defined baseline. Particularly interesting would be a moment analysis at low temperature and as a function of temperature. It must of course be borne in mind that the moment approach is only rigorous within the context of the model. In particular, the large effective line widths may in part reflect other intensity mechanisms not included in our simple treatment. Both unequal monomer force constants (see section VIII) and anharmonicity may play a significant role in determining the band contour, and both of these effects require further investigation.

Our parameter estimates, $\epsilon = -6$, $\lambda = 2.7$, permit an immediate assessment of the simple criterion for valence trapping, i.e., does the lowest potential surface have a single minimum or does it have two minima symmetrically disposed about a central potential barrier (see also Figure 7 and the discussion in section IX). The former case corresponds to a delocalized or untrapped ground state and the latter corresponds to "valence trapping". In terms of our parameters, the criterion which distinguishes the former from the latter is simply[6] $\lambda^2 \leq |\epsilon|$ vs. $\lambda^2 > |\epsilon|$ (see also section IX). Thus our parameters suggest valence trapping. *However,* using these parameters, one calculates a barrier height of only 57 cm^{-1} whereas the calculated ground state vibronic energy level is 30 cm^{-1} *above* the top of the barrier suggesting a primarily delocalized (untrapped) structure consistent with the view recently emphasized by Beattie et al.[7] and by Hush.[6] In fact, we may easily put this analysis on a quantitative basis by calculating the probability distribution ($P(q_-)$) in q_- space. We do this by squaring Φ_ν^+ (or Φ_ν^-) and integrating over electronic coordinates using eq 6. The result is

$$P_\nu^+(q_-) \equiv \int |\Phi_\nu^+|^2 d\tau_{el}$$

$$= \sum_{n,n'}^{even} r_{\nu n} r_{\nu n'} \chi_n \chi_{n'} + \sum_{l,l'}^{odd} r_{\nu l} r_{\nu l'} \chi_l \chi_{l'} \quad (37)$$

An analogous equation applies for $P_\nu^-(q_-)$ with $s_{\nu n}$ substituted everywhere for $r_{\nu n}$. Equation 37 is easily evaluated since the $r_{\nu n}$ (and $s_{\nu n}$) are obtained from the diagonalization of eq 21, and the χ_n are simply harmonic oscillator functions centered at $q_- = 0$. Calculated probability plots are shown for $\epsilon = -6$, $\lambda = 2.7$ (the C–T parameters) in Figure 4 both in the low-temperature limit (all molecules in the ground state) and at room temperature. The low-temperature case corresponds to an untrapped situation since the probability peaks at $q_- = 0$ (i.e., both Ru environments identical) and falls off smoothly as $|q_-|$ increases. At room temperature, a small degree of trapping is implied since the probability shows modest maxima near the potential well minima. In sharp contrast, we also in Figure 4 show analogous probability plots for the parameters, $\epsilon = -6$, $\lambda = 3.5$. These correspond to a potential barrier of 795 cm^{-1} and a ground vibronic energy of 210 cm^{-1}, and thus the ground state lies 585 cm^{-1} below the top of the barrier. It is seen that essentially complete trapping is predicted with virtually no temperature dependence.

If we wish to use simple resonance language,[11] then we may approximate the electron "delocalization frequency" by simply dividing the energy difference between the two lowest calculated energy levels by h. This gives frequencies of 3.9×10^{12} and 5.7×10^{10} s^{-1}, respectively, for the C–T complex and the hypothetical $\epsilon = -6$, $\lambda = 3.5$ case (assuming 500 cm^{-1} quanta).

Once more it must be stressed that our choice of ϵ and λ is within the confines of a simple model. Nevertheless, within this
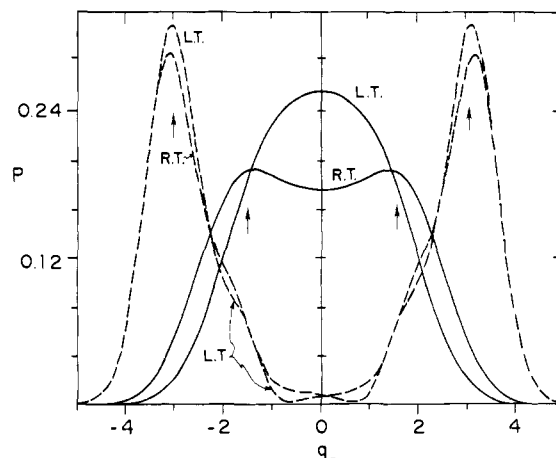
Figure 4. The calculated probability distributions in q_- space at room temperature (RT) and in the low-temperature limit (LT) for $\epsilon = -6$, $\lambda = 2.7$ (solid curves) and $\epsilon = -6$, $\lambda = 3.5$ (dashed curves). The vertical arrows designate the location of the calculated minima in the lower potential surface ($q_- = \pm 1.53$ and ± 3.05, respectively).

context, quantitative statements about valence trapping are possible since the vibronic energies and eigenfunctions of the system are calculated. It is also pleasing that the required parameters are defined quite closely by a broad, room temperature solution spectrum.

V. A Simplified Model for Unsymmetrical Mixed Valence Systems

Symmetrical mixed valence systems (A = B) are uncommon. More typically the A and B monomers are either centered about different atoms as in

$$[(NC)_5-Ru-C-N-Fe-(CN)_5]^{5+}$$

or have the same central atom but in slightly different environments as in

$$[(NC)_5-Fe-C-N-Fe-(CN)_5]^{5+}$$

Our model may be easily applied to such A $\neq$ B systems if it is assumed that, although the A and B monomers differ in zero-point potential energy ($W_M^A \neq W_M^B, W_N^A \neq W_N^B$), their environments are similar enough so that, to a good approximation, $k_M^A = k_M^B$, $k_N^A = k_N^B$, $\ell_M^A = \ell_M^B$, and $\ell_N^A = \ell_N^B$. As in the symmetrical case we further take $k_M = k_N$ for both A and B and choose coordinates so that $l_N^A = l_N^B = 0$.[12] With these assumptions, the vibronic matrix for $H^T/h\nu$ in the ψ_+,ψ_- electronic basis becomes

$$\begin{bmatrix} \frac{1}{2}(p_-^2 + q_-^2) + \epsilon & \lambda q_- + W \\ \\ \lambda q_- + W & \frac{1}{2}(p_-^2 + q_-^2) - \epsilon \end{bmatrix} \quad (38)$$

We have omitted constant terms along the diagonal and have defined W as

$$W = \frac{1}{2h\nu} \{(W_M^A + W_N^B)$$

$$- (W_N^A + W_M^B) + W^{AB}(A) - W^{AB}(B)\} \quad (39)$$

When A = B, $W = 0$. We use the same vibrational basis as in the symmetrical limit, and so in the vibronic basis the same λq_- and the same diagonal matrix elements are obtained. In addition, however, W couples the $\psi_+ \chi_n$ with the $\psi_- \chi_n$ since

$$\langle \psi_+ \chi_n(q_-) | H^T/h\nu | \psi_- \chi_{n'}(q_-) \rangle = W\delta_{nn'},$$

$$n = 0, 1, 2, \ldots \quad (40)$$
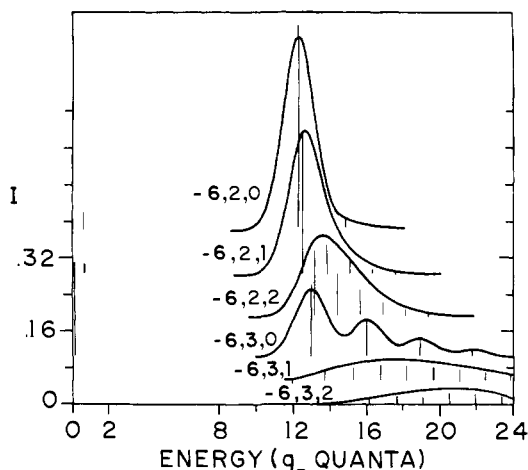
Figure 5. Calculated absorption profiles for the unsymmetrical case in the low-temperature limit. The parameters $-\epsilon$, λ, W label the bands. Spectra are synthesized analogously to those in Figure 2 using eq 43 in place of eq 28. The intensity of the low-energy infrared transition for $-6,3,2$ is negligible to the scale of the figure.

Therefore, the matrix is no longer separable into Φ^+ and Φ^- blocks. The dimension of the vibronic matrix is thus doubled.

Eigenfunctions are now in the form

$$\Phi_\nu = \sum_n (r_{\nu n}\psi_+\chi_n + r'_{\nu n}\psi_-\chi_n) \qquad (41)$$

Thus when only Φ_0 is populated and $\psi_\pm$ are nondegenerate, the A $\ne$ B analogue of eq 27 is

$$D(0 \rightarrow \nu) = \sum_{\gamma=x,y,z} |\langle\Phi_0|m_\gamma|\Phi_\nu\rangle|^2$$

$$= \sum_{\gamma=x,y,z} \left| \langle\psi_+|m_\gamma|\psi_-\rangle \sum_n r_{0n}s'_{\nu n} \right.$$

$$\left. + \langle\psi_-|m_\gamma|\psi_+\rangle \sum_n r'_{0n}s_{\nu n} \right|^2$$

$$= \sum_{\gamma=x,y,z} |\langle\psi_+|m_\gamma|\psi_-\rangle|^2 \mathscr{S}_{0\nu}^2 \qquad (42)$$

where now

$$\mathscr{S}_{0\nu} = \sum_n (r_{0n}s'_{\nu n} + r'_{0n}s_{\nu n}) \qquad (43)$$

Once again we use eq 32 to approximate the $\langle\psi_+|m_\gamma|\psi_-\rangle$ matrix elements so we obtain

$$D(0 \rightarrow \nu) = (Re/2)^2 \mathscr{S}_{0\nu}^2 \qquad (44)$$

We first consider $\mathscr{S}_{0\nu}$ in the limiting cases. When $\epsilon = 0$, but λ and W are both nonzero, no intensity is predicted for much the same reasons as in the $\epsilon = 0$, $\lambda \ne 0$ case in the symmetrical limit. Alternatively, when $\lambda = 0$ but ϵ and W are nonzero, a single line is predicted with intensity diminished from the equivalent $W = 0$ line by the factor $\epsilon^2/(W^2 + \epsilon^2)$. (This factor is most easily derived using the functions of eq 54 (see section IX)).

Figure 5 shows the pronounced effect W has on the shape of the mixed valence band when both ϵ and λ are nonzero. The band becomes higher in energy, spans more vibrational quanta, and is less intense as W increases while holding ϵ and λ constant. Thus our model accounts very nicely for the experimental observation that mixed valence bands are much broader and peak at higher energies in unsymmetrical complexes.[4]

VI. Intensity Profile and Temperature Dependence of the Mixed Valence Band in the More General Case

We now remove the restrictions that $\psi_\pm$ be nondegenerate and that only Φ_0 may be populated. If ψ_+ and ψ_- are d(ψ)-fold degenerate, H^T will block into d(ψ) equivalent blocks, each with eigenfunctions in the form of eq 41. Adding the symmetry component label, τ, to these eigenfunctions, we have

$$\Phi_\nu\tau = \sum_n (r_{\nu n}(\psi_+\tau)\chi_n + r'_{\nu n}(\psi_-\tau)\chi_n) \qquad (45)$$

Using the same arguments which led to eq 32, we obtain

$$\langle\psi_+\tau'|m_\gamma|\psi_-\tau\rangle = \delta_{\gamma z}\delta_{\tau\tau'} \langle\psi_+\tau|m_z|\psi_-\tau\rangle$$
$$= \delta_{\gamma z}\delta_{\tau\tau'}(Re/2) \qquad (46)$$

Substituting eq 45 into eq 25 gives

$$D(\nu' \rightarrow \nu) = \sum_\gamma \sum_{\tau,\tau'} \frac{(N_{\nu'\tau'} - N_{\nu\tau})}{\left[\sum_{\nu',\tau'} N_{\nu'\tau'}\right]} |\langle\Phi_{\nu'}\tau'|m_\gamma|\Phi_\nu\tau\rangle|^2$$

$$= \left(\sum_\gamma \frac{1}{\mathrm{d}(\psi)} \sum_{\tau,\tau'} |\langle\psi_+\tau'|m_\gamma|\psi_-\tau\rangle|^2\right)$$

$$\times \frac{[\exp(-E_{\nu'}/kT) - \exp(-E_\nu/kT)]}{\left(\sum_{\nu'} N_{\nu'}\right)} \mathscr{S}_{\nu'\nu}^2 \qquad (47)$$

and then using eq 46 we have

$$D(\nu' \rightarrow \nu) \cong (Re/2)^2$$

$$\times \frac{[\exp(-E_{\nu'}/kT) - \exp(-E_\nu/kT)]}{N} \mathscr{S}_{\nu'\nu}^2 \qquad (48)$$

and

$$\mathscr{S}_{\nu'\nu} \equiv \sum_n (r_{\nu'n}s'_{\nu n} + r'_{\nu'n}s_{\nu n}) \qquad (49)$$

This expression may be used to calculate the band profile as a function of temperature.

In Appendix 1 we show that the theoretical absorption profile may be written as a function of the energy, E, and used to evaluate moments.

VII. Inclusion of Spin–Orbit Coupling

Somewhat surprisingly, inclusion of spin–orbit coupling does not change the absorption bandshape predicted by our model for the cases outlined above. This result is due to the stringent selection rules (eq 32 and 46) governing $\langle\psi_+|m_\gamma|\psi_-\rangle$ matrix elements in our approximation. Our earlier discussion of these matrix elements shows, for example, that if τ and τ' are spin-orbit states arising from ψ_A^M then

$$\langle\Gamma(\psi_A^M)\tau|m_z|\Gamma'(\psi_A^M)\tau'\rangle \cong -m(Re/2)\delta_{\Gamma\Gamma'}\delta_{\tau\tau'} \qquad (50)$$

Thus the same number of transitions are allowed from the lowest level of the spin–orbit split ground state as in the zero spin–orbit coupling limit. Moreover, the transitions have the same energies and intensities in both cases.

VIII. Nonequivalent Force Constants: $k_M \ne k_N$

When the force constant k differs in the M and N oxidation states in the symmetrical (A = B) limit, the matrix eq 17 becomes the matrix eq 51. The vibronic matrix is no longer separable in Q_+ and Q_- since the $\frac{1}{2}(k_M - k_N)$-Q_+Q_- term couples $\psi_+\chi_n(Q_-)\chi_p(Q_+)$ states with $\psi_-\chi_{n'}(Q_-)\chi_{p'}(Q_+)$ states which differ in one quantum of $\nu(Q_-)$ ($\Delta n = 1$) and in one quantum of $\nu(Q_+)$ ($\Delta p = 1$). This has important implications with respect to our intensity profile calculation. When the Q_+ system is separable, the ground state at low temperatures will be a pure $p = 0$ state with respect to

$$\begin{bmatrix} \left\{ \dfrac{P_+^2}{2M} + \dfrac{\ell}{\sqrt{2}}Q_+ + \dfrac{1}{2}\left(\dfrac{k_N + k_M}{2}\right)Q_+^2 \right. \\ \left. + \dfrac{P_-^2}{2M} + \dfrac{1}{2}\left(\dfrac{k_N + k_M}{2}\right)Q_-^2 \right\} + W_s \\ \\ \dfrac{\ell Q_-}{\sqrt{2}} + \dfrac{(k_M - k_N)}{2}Q_+Q_- \end{bmatrix} \quad \begin{matrix} \dfrac{\ell Q_-}{\sqrt{2}} + \dfrac{(k_M - k_N)}{2}Q_+Q_- \\ \\ \left\{ \dfrac{P_+^2}{2M} + \dfrac{\ell}{\sqrt{2}}Q_+ + \dfrac{1}{2}\left(\dfrac{k_N + k_M}{2}\right)Q_+^2 \right. \\ \left. + \dfrac{P_-^2}{2M} + \dfrac{1}{2}\left(\dfrac{k_N + k_M}{2}\right)Q_-^2 \right\} - W_s \end{matrix} \qquad (51)$$

displaced Q_+ oscillator states, $\chi_p'(Q_+)$. Thus electric-dipole transitions are allowed only to other vibronic states with $p = 0$ in $\chi_p'(Q_+)$. On the other hand, in the $k_M \neq k_N$ case, the ground state is no longer a pure $\chi_p'(Q_+) = \chi_0'(Q_+)$ state, and the selection rule in p breaks down. Thus we would expect the bandshape to be blurred by these additional allowed lines. We therefore suggest unequal force constants as an important contributing factor to the large effective line width in mixed valence spectra. We are currently investigating the consequences of including unequal force constants in the model.

IX. Potential Energy Surfaces

In this section, we discuss some properties of the potential surfaces implicit in our model. Pictures of such surfaces offer important physical insight into the mixed valence problem, but we shall also stress the pitfalls inherent in attempting to use such pictures in general to predict, except in a very qualitative way, absorption profiles. The situation will be found closely analogous to the Jahn–Teller problem. Our discussion should also make clearer the relation of the present treatment to earlier discussions[4-7] which focus on the potential surfaces but do not attempt quantitative band profile calculations.

Equations for the potential surfaces relevant to mixed valence intensities are obtained very easily by diagonalization of the potential energy part of eq 38:

$$E_1 = \frac{1}{2}q_-^2 - (\epsilon^2 + (\lambda q_- + W)^2)^{1/2}$$

$$E_2 = \frac{1}{2}q_-^2 + (\epsilon^2 + (\lambda q_- + W)^2)^{1/2} \qquad (52)$$

The electronic eigenfunctions associated with these surfaces are easily found by substituting E_1 and E_2 back into this part of eq 38. We find

$$\psi_1(q_-) = \frac{1}{N(q_-)}$$
$$\times \{-(\epsilon - \sqrt{\epsilon^2 + (\lambda q_- + W)^2})\psi_+ - (\lambda q_- + W)\psi_-\}$$

$$\psi_2(q_-) = \frac{1}{N(q_-)}$$
$$\times \{(\lambda q_- + W)\psi_+ - (\epsilon - \sqrt{\epsilon^2 + (\lambda q_- + W)^2})\psi_-\} \qquad (53)$$

where

$$N(q_-) = [(\lambda q_- + W)^2$$
$$+ (\epsilon - \sqrt{\epsilon^2 + (\lambda q_- + W)^2})^2]^{1/2} \qquad (54)$$

and $\psi_\pm$ are defined by eq 16. These functions are eigenfunctions of $H_{el}(r,Q)$ which includes all parts of H^T other than the T_n (the "dynamic") terms. Thus we are now writing eq 1 in the form

$$H^T = H_{el}(r,Q) + (T_n^A + T_n^B + T_n^{AB}) \equiv H_{el}(r,Q) + T_n$$

In Jahn–Teller problems, E_1, E_2 and ψ_1, ψ_2 are called the solutions to the "static" problem.

Since obtaining ψ_1 and ψ_2 above is so simple, the reader may wonder why we do not proceed from the "static" solutions above to solve the full (the "dynamic") Hamiltonian, H^T. The answer is that *in general ψ_1 and ψ_2 are sensitive functions of* q_-; thus they do not commute with the T_n and they may not in general be used as electronic functions when making the Franck–Condon approximation for electronic matrix elements. The full dynamic problem must be solved to calculate absorption profiles. It is much easier to do that, as we do earlier, starting from eq 21 or 38.

In the special cases where ϵ and λ are not *simultaneously* nonzero, ψ_1 and ψ_2 *are* q_- independent. Then the electronic and nuclear problems *are* separable and it is straightforward to predict the absorption profile in our model using conventional arguments. *In these special cases*, the solutions are simply

$$\Phi_{m'} = \psi_1 \chi_{m'}$$
$$\Phi_m = \psi_2 \chi_m \qquad (55)$$

where $\chi_{m'}$ and χ_m are harmonic oscillator solutions to

$$(\tfrac{1}{2}p_-^2 + E_1)\chi_{m'} = E_{1,m'}\chi_{m'}$$
$$(\tfrac{1}{2}p_-^2 + E_2)\chi_m = E_{2,m}\chi_m \qquad (56)$$

since when ϵ and λ are not *both* nonzero, the potential (E_1 or E_2) *is* harmonic (to the usual first approximation). Thus we can derive the statements we make in earlier sections concerning the limiting cases from these equations alone. This is straightforward since harmonic oscillator solutions are well known. The solutions, eq 55, are identical with those of eq 41 but are expressed in a different basis. In Figure 6 we show the potential energy surfaces for selected limiting cases, give equations for E_1, E_2, ψ_1, and ψ_2, and indicate the absorption profile using the above method.

When both $\epsilon \neq 0$ *and* $\lambda \neq 0$ (the chemically interesting cases!), the potential is no longer harmonic, and ψ_1 and ψ_2 are q_- dependent and do not commute with T_n. Potential surfaces are illustrated in Figure 7 for three such cases. When $\lambda^2 \leq |\epsilon|$, E_1 has a single minimum at $q_- = 0$ as does E_2 in all cases. When $\lambda^2 > |\epsilon|$, the lower (E_1) curve has two minima, at $q_- = \pm(\lambda^4 - \epsilon^2)^{1/2}/\lambda$. While it is easy to see qualitatively that as λ gets large compared to ϵ the absorption band will become broader and less intense, *quantitative predictions require diagonalization of H^T*. This is easily accomplished as outlined in earlier sections.

X. Conclusions

While our model for mixed valence systems is a simplified one, we believe that it contains the most important features of the real systems. As far as we know, it has permitted the first calculation of the actual vibronic stationary states of mixed valence systems. We consider such calculations an essential first step in obtaining meaningful absorption profiles. The model is successful in explaining both the narrow, asymmetric absorption band in the symmetrical Creutz–Taube complex and the broader, more diffuse mixed valence bandshape observed in unsymmetrical complexes. Furthermore, the pa-
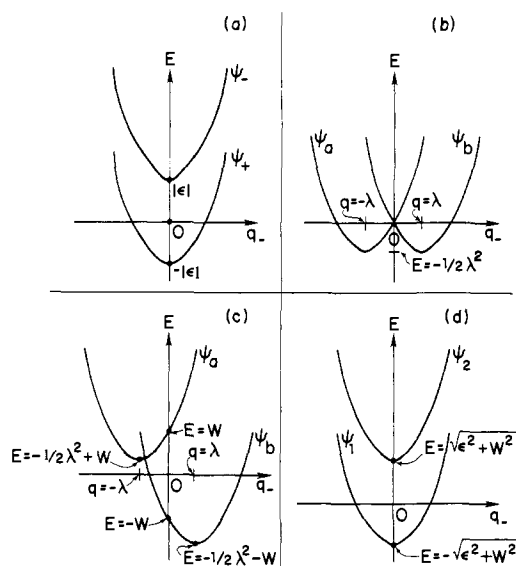
Figure 6. Potential energy surfaces for selected limiting cases: (a) $\epsilon < 0$, $\lambda = W = 0$; $E_{1,2} = (q_-^2/2) \mp |\epsilon|$; spectrum one line at energy $2|\epsilon|$; (b) $\lambda > 0$, $\epsilon = W = 0$; $E_{1,2} = (q_-^2/2) \mp \lambda q_-$; no spectrum since $\langle \psi_a | \psi_b \rangle \approx 0$; (c) $\lambda > 0$, $W > 0$, $\epsilon = 0$; $E_{1,2} = (q_-^2/2) \mp (W + \lambda q_-)$; no spectrum since $\langle \psi_a | \psi_b \rangle \approx 0$; (d) $\epsilon < 0$, $W > 0$, $\lambda = 0$; $E_{1,2} = (q_-^2/2) \mp \sqrt{\epsilon^2 + W^2}$; ψ_1, ψ_2, N given by eq 54; spectrum one line at energy $2|\epsilon|$ with intensity reduced by factor $[\epsilon^2/(W^2 + \epsilon^2)]$ with respect to (a).

rameters in the model are directly related to the properties of the monomeric units. Thus λ is explicitly related to the difference in bond lengths of the monomer units in different oxidation states (Figure 1), and so, for example, the very small difference[13] in equilibrium bond lengths between $Ru(NH_3)_6^{2+}$ and $Ru(NH_3)_6^{3+}$ correlates well with the narrow C-T bandwidth. The frequency of the coupling vibration, ν_-, may be approximated as the average of the totally symmetric vibration of the two monomers. The exciton coupling parameter ϵ may be calculable via the multipole expansion approach which has been extensively used in explaining the properties of "Davydov split" dimers.[14]

Finally, the model allows direct comparison of experimental and theoretical bandshapes as a function of ϵ, λ, W, and the temperature. Furthermore, the moment equations derived in the Appendix show that for the zeroth and first moments such comparisons can be made largely independently of a knowledge of vibronic line shapes. The model may also be useful in the discussion of electron transfer kinetics since the vibronic problem is solved explicitly in terms of well-defined parameters.

In this paper we have limited our discussion to absorption bands. A more challenging task which we have recently begun is an extension of the model to make possible meaningful magnetic circular dichroism (MCD) calculations. In our present model, only the m_z matrix element is nonzero (eq 32 or 46) whereas the presence of MCD requires nonzero m_x, m_y transitions as well. Güdel and Krausz[15] have measured the MCD (and absorption spectra) of a variety of mixed valence complexes in poly(vinyl alcohol) films at low temperature. The MCD of the mixed valence transitions is very weak relative to the absorption, in qualitative accord with our model which predicts zero MCD to a first approximation. On the other hand, MCD spectra are clearly measurable and have quite distinctive patterns. Such spectra may be useful as a diagnostic tool in complex systems such as iron sulfur proteins where mixed valence couples are often in question. Initial measurements on model compounds such as the elegant ones prepared by Holm and co-workers[16] might be illuminating in this regard.
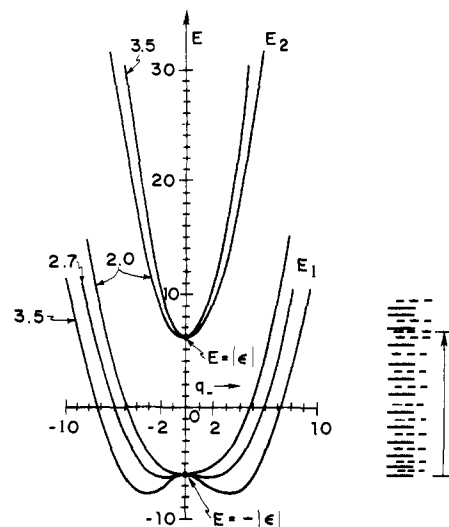
Figure 7. Upper (E_2) and lower (E_1) potential surfaces (in units of q_- quanta) for $\epsilon = -6$, $\lambda = 2.0, 2.7, 3.5$. E_2 is omitted for $\lambda = 2.7$. The energies of the lower lying vibronic levels for $\lambda = 2.7$ are shown to the right; the solid lines have symmetry (+) and the dashed lines symmetry (−). The vertical arrow shows the strongest single transition in the low-temperature limit for $\lambda = 2.7$.

Appendix. Moments

In Figures 2, 3, and 5 we showed synthesized theoretical absorption profiles assuming that each vibronic line has a Gaussian line shape with identical Δ. Another way of making a comparison between theoretical and experimental bandshapes is to use moment analysis.[17] Though not affording a simple visual comparison, this method is less dependent on specific line shape assumptions.

If $\alpha(E)$ is a function describing the absorption profile (either theoretical or experimental), the nth moment of $\alpha(E)$ about a chosen energy, E_0, is defined as

$$\langle \alpha \rangle_n^{E_0} = \int_{band} \alpha(E)(E - E_0)^n dE \qquad (A1)$$

Thus the zeroth moment is simply the integral of $\alpha(E)$. We define $E_0 = \bar{E}$ where $\bar{E}$ is the value of E for which $\langle \alpha \rangle_1^{E_0} = 0$. Thus

$$\bar{E} = \frac{\int \alpha(E) E dE}{\int \alpha(E) dE} \qquad (A2)$$

and

$$\langle \alpha \rangle_n^{\bar{E}} \equiv \int \alpha(E)(E - \bar{E})^n dE \qquad (A3)$$

Our theoretical absorption profile may be described by the function

$$\alpha(E) = \sum_\alpha \sum_a \sum_j \frac{(N_a - N_j)}{N} |\langle a | m_\alpha | j \rangle|^2 f_{aj}(E) \qquad (A4)$$

where $f_{aj}(E)$ is a line shape function for which

$$\int f_{aj}(E) dE = 1$$

If $f_{aj}(E) = \delta(E_j - E_a - E)$, then

$$\int f_{aj}(E) E^n dE = (E_j - E_a)^n$$

and substituting eq A4 into eq A3 gives

$$\langle\alpha\rangle_n^{\overline{E}} = \sum_{\gamma}\sum_a\sum_j \frac{(N_a - N_j)}{N}$$
$$\times |\langle a|m_\gamma|j\rangle|^2[(E_j - E_a) - \overline{E}]^n \quad (A5)$$

For $n = 0$ or 1, any function, $f_{aj}(E)$, symmetrical about $(E_j - E_a)$ will give eq A5. The sum over a is over all populated (ground) states and that over j is over all states contributing to the band of interest. In our case, a and j are vibronic eigenstates of H^T such as those of eq 24 and 45. Thus they are diagonal in H^T and so

$$\begin{aligned} E_a &= \langle a|H^T|a\rangle \\ E_j &= \langle j|H^T|j\rangle \end{aligned} \quad (A6)$$

Thus from eq A5, A6, and 45 we obtain

$$\langle\alpha\rangle_0 = d_0\sum_{\nu'}\sum_\nu{}' \frac{(N_{\nu'} - N_\nu)}{N'} \mathcal{S}^2_{\nu'\nu}$$

$$\langle\alpha\rangle_1^{\overline{E}} = 0$$

$$\overline{E} = \frac{d_0}{\langle\alpha\rangle_0}\sum_{\nu'}\sum_\nu{}' \frac{(N_{\nu'} - N_\nu)}{N'} \mathcal{S}^2_{\nu'\nu}(E_\nu - E_{\nu'})$$

$$\langle\alpha\rangle_2^{\overline{E}} = d_0\sum_{\nu'}\sum_\nu{}' \frac{(N_{\nu'} - N_\nu)}{N'} \mathcal{S}^2_{\nu'\nu}(E_\nu - E_{\nu'})^2 \quad (A7)$$

where

$$N_{\nu'} = \exp(-E_{\nu'}/kT), \quad N' = \sum_{\nu'}N_{\nu'}$$

and

$$d_0 = \frac{1}{\lambda(\psi)}\sum_\gamma\sum_{\tau,\tau'}|\langle\psi_+\tau'|m_\gamma|\psi_-\tau\rangle|^2 \cong (Re/2)^2 \quad (A8)$$

The sum over ν is over all states for which $E_\nu > E_{\nu'}$. We assume that all populated vibronic states are associated with the $\lambda(\psi)$-fold degenerate states ψ_+ and ψ_-.

These zeroth, first, and second moments are related to the integrated intensity, the mean energy, and the half-width, respectively, of the absorption band.[17] Experimental moments are easily calculated by integrating the experimental dispersion using eq A3. They may then be compared as a function of temperature with theoretical moments (eq A7) based on $E_{\nu'}$, E_ν, and $\mathcal{S}_{\nu'\nu}$ factors calculated for particular ϵ, λ, and W sets. This comparison should be valid for $n = 0$, 1. For $n = 2$, it should be valid if the line width, Δ, is much less than the mixed valence bandwidth.

References and Notes

(1) Department of Chemistry, Randolph-Macon Woman's College, Lynchburg, Va. 24504.
(2) (a) A. Ludi and H. U. Güdel, *Struct. Bonding (Berlin)*, **14**, 1 (1973); (b) M. B. Robin and P. Day, *Adv. Inorg. Chem. Radiochem.*, **10**, 247 (1967); (c) G. Allen and N. S. Hush, *Prog. Inorg. Chem.*, **8**, 357 (1967).
(3) (a) C. Creutz and H. Taube, *J. Am. Chem. Soc.*, **91**, 3988 (1969); (b) *ibid.*, **95**, 1086 (1973).
(4) N. S. Hush, *Prog. Inorg. Chem.*, **8**, 391 (1967).
(5) N. S. Hush, *Electrochim. Acta*, **13**, 1005 (1968).
(6) N. S. Hush, *Chem. Phys.*, **10**, 361 (1975).
(7) J. K. Beattie, N. S. Hush, and P. R. Taylor, *Inorg. Chem.*, **15**, 992 (1976).
(8) R. L. Fulton and M. Gouterman, *J. Chem. Phys.*, **35**, 1059 (1961).
(9) R. L. Fulton and M. Gouterman, *J. Chem. Phys.*, **41**, 2280 (1964).
(10) H. U. Güdel, personal communication.
(11) L. Pauling and E. B. Wilson, Jr., "Introduction to Quantum Mechanics, McGraw-Hill, New York, N.Y., 1935, Section 41.
(12) In an octahedral complex, $ML_6^{n\pm}$, $\nu_1(a_{1g}) = \sqrt{k/m_L}$ where k is the force constant and m_L is the mass of the ligand. Consequently, if the ν_1 are known (for example, from Raman data) for the monomers, the validity of the approximation $k_M^A = k_M^B = k_N^A = k_N^B$ can be assessed.
(13) W. P. Griffith, *J. Chem. Soc. A*, 899 (1966).
(14) See for example, D. P. Craig and S. H. Walmsley, "Excitons in Molecular Crystals", W. A. Benjamin, New York, N.Y., 1968.
(15) H. U. Güdel and E. R. Krausz, unpublished data.
(16) M. A. Bobrik, K. O. Hodgson, and R. H. Holm, *Inorg. Chem.*, **16**, 1851 (1977), and references cited therein.
(17) C. H. Henry, S. E. Schnatterly, and C. P. Slichter, *Phys. Rev. Sect. A*, **137**, 583 (1965).
(18) S. B. Piepho *et al.*, *Chem. Phys. Lett.*, in press.

Interaction of Walsh Orbitals in Trishomocycloheptatrienes and Related Hydrocarbons

Jens Spanget-Larsen, Rolf Gleiter,* Michael R. Detty, and Leo A. Paquette*

Contribution from the Institut für Organische Chemie der Technischen Hochschule Darmstadt, D-6100 Darmstadt, West Germany, and the Department of Chemistry, The Ohio State University, Columbus, Ohio 43210. Received July 14, 1977

Abstract: The photoelectron (PE) spectra of *syn-* and *anti-*3,5-bishomocycloheptatriene (**1** and **2**), *syn-* and *anti-*1,5-bishomocycloheptatriene (**3** and **4**), and *syn,syn-*, *anti,anti-*, and *anti,syn-*trishomocycloheptatriene (**5**, **6**, and **7**) have been recorded. The first bands of their spectra have been assigned to ionization from molecular orbitals (MOs) derived from the highest occupied Walsh orbitals of the cyclopropane rings and the π orbital of the ethylenic double bond. This analysis is based on a zero differential overlap (ZDO) model and substantiated by the results of semiempirical calculations. An important feature of the ZDO model is the admixture of "radially" oriented components into the highest occupied "tangential" Walsh orbitals which is necessary to improve the description of the conformationally dependent interaction between linked cyclopropyl groups.

Introduction

The interaction between the Walsh orbitals of three cyclopropane rings has been studied recently in the case of diademane.[1] In this example, the dihedral angle between the cyclopropane units is approximately zero and the conjugative interaction between Walsh orbitals composed of "tangentially"

oriented 2p atomic orbitals (AOs) is a maximum. On the basis of photoelectron (PE) spectroscopic results the resonance integral between linked 2p AOs of two adjacent eclipsed cyclopropane rings was found to be -1.73 eV.

In this paper, an evaluation is made of those hydrocarbons derived from cycloheptatriene in which the dihedral angles between the cyclopropane units deviate markedly from zero.